ADVANCED MATERIALS INTERFACES
www.advmatinterfaces.de

# Resolving Oxidation States and *X*–site Composition of Sn Perovskites through Auger Parameter Analysis in XPS

*Alexander Wieczorek, Huagui Lai, Johnpaul Pious, Fan Fu,* and Sebastian Siol**

**Reliable chemical state analysis of Sn semiconductors by XPS is hindered by the marginal observed binding energy shift in the Sn 3d region. For hybrid Sn-based perovskites especially, errors associated with charge referencing can easily exceed chemistry-related shifts. Studies based on the modified Auger parameter $\alpha'$ provide a suitable alternative and have been used previously to resolve different chemical states in Sn alloys and oxides. However, the meaningful interpretation of Auger parameter variations on Sn-based perovskite semiconductors requires fundamental studies. In this work, a comprehensive Auger parameter study is performed through systematic compositional variations of Sn halide perovskites. It is found that in addition to the oxidation state, $\alpha'$ is highly sensitive to the composition of the halide site, inducing shifts of up to $\Delta\alpha' = 2$ eV between $ASnI_3$ and $ASnBr_3$ type perovskites. The reported dependencies of $\alpha'$ on the Sn oxidation state, coordination and local chemistry provide a framework that enables reliable tracking of degradation as well as *X*-site composition for Sn-based perovskites and related compounds. The higher robustness and sensitivity of such studies not only enables more in-depth surface analysis of Sn-based perovskites than previously performed, but also increases reproducibility across laboratories.**

## 1. Introduction

Across a wide range of applications, semiconductors based on Sn are being investigated. Besides kesterites (e.g., $Cu_2ZnSnS_4$),[1] chalcogenides (e.g., SnSe)[2] and group IV alloys (e.g., GeSn),[3] Sn halide perovskites have peaked interest for optoelectronic applications.[4] Their composition follows the formula $ASnX_3$ where typically A = $Cs^+$, methylammonium ($MA^+$), formamidinium ($FA^+$) and X = $I^-$, $Br^-$, $Cl^-$. Furthermore, they are classified by their perovskite crystal structure (**Figure 1**a). Their lower toxicity compared to their more established $APbX_3$ counterparts and relatively narrower yet tunable bandgap make them attractive candidates for a range of optoelectronic applications.[5] However, the facile oxidation of the Sn(II) species to Sn(IV) compounds severely limits their lifetime, especially under ambient conditions.[6]

The development of Sn-based semiconductors necessitates a reliable determination of the chemical state of the constituent elements. X-ray photoelectron spectroscopy (XPS) is an important tool in this regard to conduct research on novel energy materials and devices.[7,8]

Typically, these studies are based on the observation of the core level photoelectron emission features and their position on the binding energy ($E_b$) scale. To counteract charging effects, referencing based on adventitious carbon is often performed. However, this results in a typical inaccuracy of ±0.2 eV, whereas even errors of >1 eV have been observed.[9]

For many Sn compounds with different Sn oxidation states and compositions, the main Sn 3d core level emission exhibits only minimal $E_b$ shifts, which lie below this error range. Consequently, probing degradation as well as assigning the effects of compositional changes and additives to the surface chemistry of Sn-based perovskites with conventional XPS can be challenging.

In addition, shifts on the binding energy scale not originating from chemical bonds are especially pronounced for semiconductors (Figure 1b). Similar to effects observed in UPS,[10] excitation during measurement with an X-Ray source may induce photovoltages,[11] resulting in surface band bending. Surface charges, e.g., induced by ionic additives, may lead to similar effects that originate from the resulting space charge and not the bonding to the additive itself.[12] Consequently, a probing depth-dependent shift is induced, which may further inhibit reliable charge referencing. Similarly, changes in the materials' work function (e.g., due to differences in doping) would also result in changes of the absolute binding energies for an otherwise identical material.

For chemical state analysis of Sn, XPS analysis based on the modified Auger parameter (AP) concept offers an effective alternative to distinguish different chemical states.[13] This approach relies on the observation of both the photoelectrons (i.e., Sn 3d) and Auger electrons (i.e., Sn MNN).

A. Wieczorek, S. Siol
Laboratory for Surface Science and Coating Technologies
Empa–Swiss Federal Laboratories for Materials Science and Technology
Ueberlandstrasse 129
Duebendorf CH-8600, Switzerland
E-mail: sebastian.siol@empa.ch
H. Lai, J. Pious, F. Fu
Laboratory for Thin Films and Photovoltaics
Empa–Swiss Federal Laboratories for Materials Science and Technology
Ueberlandstrasse 129
Duebendorf CH-8600, Switzerland
E-mail: fan.fu@empa.ch
The ORCID identification number(s) for the author(s) of this article can be found under https://doi.org/10.1002/admi.202201828.



**DOI: 10.1002/admi.202201828**

 

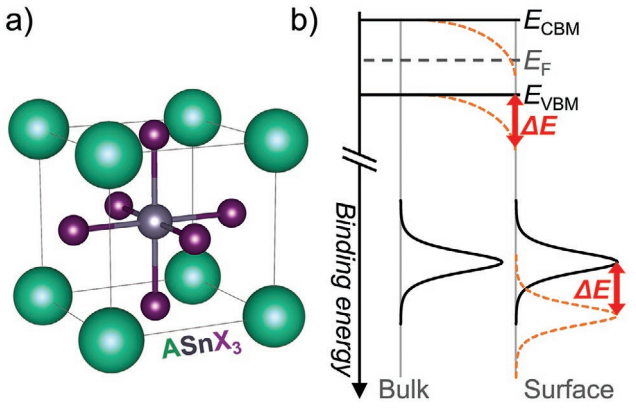


**Figure 1.** a) Perovskite crystal structure. b) Schematic of the band positions and core-level features observed using XPS with (orange dashed) or without (black solid) surface band bending effects. Shown are the valence band maximum $E_{VBM}$, conduction band minimum $E_{CBM}$ and Fermi level position $E_F$. A change of the surface potential $\Delta E$ (i.e., the Fermi level position) due to differential charging or surface photo voltages results in surface band bending and consequently in a shift of the observed XPS features, depending on the probing depth.

The modified Auger parameter $\alpha'$ can be calculated according to

$$\alpha' = E_{kin}\left(\text{Sn } M_4N_{4,5}N_{4,5}\right) + E_b\left(\text{Sn } 3d_{5/2}\right) \quad (1)$$

where $E_{kin}$(Sn $M_4N_{4,5}N_{4,5}$) denotes the kinetic energy of the Sn $M_4N_{4,5}N_{4,5}$ feature maximum and $E_b$(Sn $3d_{5/2}$) denotes the binding energy of the Sn $3d_{5/2}$ feature maximum.[14]

Since the AP is only determined from the relative positions of these features to another, the AP is insensitive to charging effects and erroneous binding energy calibration. Furthermore, the Auger emission is more sensitive to changes in the local chemical environment than the photoelectron emission, due to the double core-hole final state in the Auger process.[15] Using this additional feature may therefore increase the shifts observed due to altered chemical states. This holds especially true for the Sn MNN Auger emission feature resulting from valence shell transitions that is accessible using standard XPS excitation sources (i.e., Al k$\alpha$).

AP shifts $\Delta\alpha'$ can be described as

$$\Delta\alpha' = 2\left(\Delta R^a + \Delta R^{ea}\right) \quad (2)$$

where $\Delta R^a$ denotes differences in the valence charge of the core-ionized atom and $\Delta R^{ea}$ denotes differences in the extra-atomic relaxation energy.[15]

The valence charge may be influenced by the oxidation state whereas increased oxidation states typically result in decreased $\Delta R^a$ and thus decreased $\Delta\alpha'$. Additionally, the valence charge may be lowered through more electronegative nearest-neighbors, likewise resulting in decreased $\Delta R^a$.

Using the electrostatic model introduced by Moretti,[16] the extra-atomic relaxation affecting $\Delta R^{ea}$ results from the coordination number, the distance and electronic polarizability of the core-ionized atom's nearest-neighbors. As reported by Biesinger et al.,[17,18] increased covalency of the nearest-neighbor bonds may result in increased $\Delta R^{ea}$ for a core-ionized cation as shared electrons result in increased polarizability. As the electronegativity also affects the covalency, it alters both $\Delta R^a$ and $\Delta R^{ea}$. For semiconductors specifically, extra-atomic relaxation often dominates changes of the AP.[15]

While first attempts have been made to use the AP approach for Sn compounds,[19] there is a lack of systematic studies on the effects of oxidation state and X-site composition for Sn-based perovskites specifically. Since the aforementioned various factors govern the resulting AP value,[20] empirical studies on reference samples may help to unravel each contributing factor and understand more complex samples.[21]

In this work we perform AP analysis on a comprehensive set of reference compounds typically found in literature. The perovskite structure for each sample was confirmed by XRD, while the transfer into the XPS measurement system was performed in inert-gas atmosphere. Based on this systematic study, we identified a high sensitivity of the AP on Sn—X bonds. This enables more in-depth and robust chemical state analysis via XPS than studies that are based on the observation of the photoelectron emission alone. In addition, the results from this work can be used by other researchers and groups to track and resolve the Sn chemical state in related compounds. Finally, the methods presented here are applicable for interface studies on perovskites devices providing additional and valuable insights for interface engineering.[22]

## 2. Results and Discussion

To obtain high-quality perovskite reference samples representing the typical compositional space for optoelectronics applications, we prepared $ASnX_3$ type perovskites with A = $Cs^+$, $FA^+$, $MA^+$ and X = $Br^-$, $I^-$. Preparation and transfer of samples to the XPS was conducted under inert gas to prevent the formation of surface oxides. Short-term measurements (<1 min) of the Sn 3d core level were performed before and after each long-term measurement (≈30 min) to ensure the observed features remained stable during these measurements (Figure S1, Supporting Information). This ensured that the reported APs reflect the chemical states of pristine samples instead of aged samples with surface oxides or X-ray induced damage. Quantification based on XPS indicated, that the stoichiometry is preserved for each sample when comparing pristine areas (Table S2, Supporting Information) and those previously subjected to long-term measurements (≈30 min) (Table S3, Supporting Information). To confirm the successful conversion of the precursors to the perovskite phase, each film was analyzed using X-ray diffraction (XRD) after the XPS analysis.

As evident from the XPS measurements of the Sn 3d regions for $MASnI_3$ and $FASnBr_3$, no clear shift can be observed for the Sn $3d_{5/2}$ feature between these compounds (**Figure 2**a). These results are well in alignment for the minor reported shifts of <0.2 eV even between SnO (i.e., Sn(II)) and $SnO_2$ (i.e., Sn(IV)) from literature.[24,25] In contrast, shifts of >2.0 eV can be observed for the maxima of the $M_4N_{4,5}N_{4,5}$ emissions (Figure 2b) in alignment with the increased sensitivity of the Auger emission to the local chemical environment of Sn. While the determination of the Sn chemical state on the Auger emission alone may thus appear attractive, the absolute values on

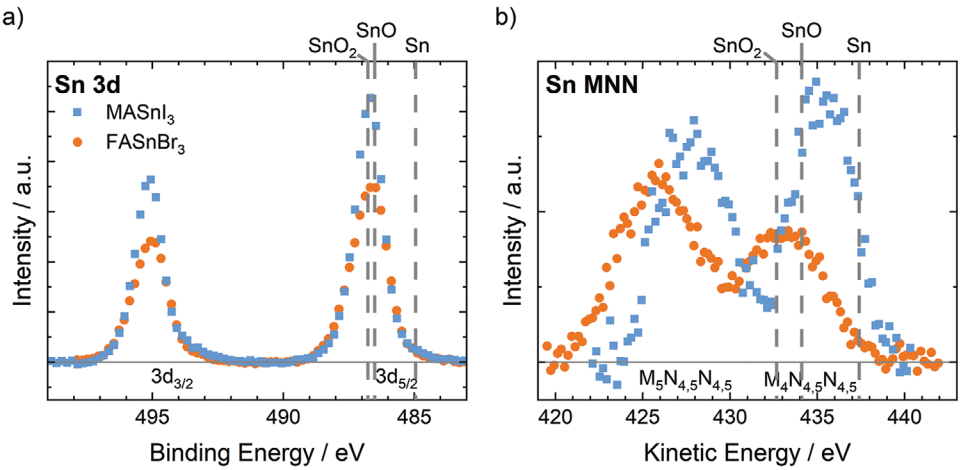


**Figure 2.** Representative spectra of the a) Sn 3d core level and b) Sn MNN Auger electron emission of $MASnI_3$ and $FASnBr_3$ measured by XPS. Vertical lines show the peak position of Sn, SnO, and $SnO_2$ that were extracted from the NIST database.[23]

the kinetic energy ($E_{kin}$) scale remain dependent on external charge referencing as well as potential surface band bending. In contrast, the AP is largely independent from the Fermi level position and work function at the surface.

Deconvolution of the Auger emission is often impractical, as well as ambiguous, due to the complexity of the underlying physical processes, resulting in a large amount of overlapping Auger electron features.[26] Consequently, as often applied for Sn alloys and oxides,[27–29] we performed the AP analysis based on the maximum of the Sn $M_4N_{4,5}N_{4,5}$ feature. The same applies for the Sn 3d core level. Especially, when binding energy shifts between different compounds are minute, peak fitting with multiple components separated by minor energy shifts can add ambiguity to the results and hinder reproducibility of the results between different groups. Here we used the binding energy of the most pronounced Sn $3d_{5/2}$ feature maximum.

This relationship can be visualized by a Wagner plot (**Figure 3**), where $E_b$(Sn $3d_{5/2}$) and $E_{kin}$(Sn$M_4N_{4,5}N_{4,5}$) are plotted against each other.[30] As a result, $\alpha'$ as the crucial value appears as a diagonal line in this graph. Charging effects may only shift the data points along these diagonal lines. Furthermore, as evident from the reference values of SnO and $SnO_2$ in the graph, shifts in the AP are mostly originating from the shifts of their $E_{kin}$(Sn $M_4N_{4,5}N_{4,5}$) values. Since this approach relies on the comparison of features across wide energy ranges, a careful calibration of the linearity of the kinetic energy scale of the instrument is critical (see Note S1, Supporting Information).

We performed detailed XPS analysis on a large number of reference compounds and calculated $\alpha'$ of Sn (Equation 1). The resulting values for all reference Sn-based perovskites are displayed in a single Wagner plot (**Figure 4**).

Most notably a clear clustering is observed depending on the choice of halide, allowing to resolve trends beyond those observed based on the Sn 3d feature alone. For all $ASnI_3$ type perovskites, the AP was clustered at $\alpha' \approx 922$ eV. Strikingly, $ASnBr_3$ type perovskites exhibited a clustering $\alpha' \approx 920$ eV, resulting in a shift of $\Delta\alpha' \approx 2$ eV compared to $ASnI_3$ type perovskites. A minor shift to lower AP of $\Delta\alpha' < 1$ eV was observed for $SnI_2$ compared to the respective $ASnI_3$ type perovskites. This could be due to a change in the coordination and valence charge of Sn in the respective structures. However, a similar shift was not evident for $SnBr_2$ compared to $ASnBr_3$ type perovskites. From the present data, it is unclear if this result could be influenced by the minor Sn(0) fraction that was observed for $SnBr_2$. Therefore, a clear trend for $\alpha'$ could not be established when moving from metal halides to their respective perovskites.

More information on the origin of this metallic fraction and similar effects in B–site alloyed perovskites can be found in the Note S2 (Supporting Information).

As previously introduced, shifts of $\alpha'$ depend both on the valence charge of the core-ionized atom as well as the local chemical environment, i.e., the nearest neighbors.[15] Due to the identical preparation conditions and lack of significant Sn(0) formation for $ASnI_3$ and $ASnBr_3$ type perovskites, the Sn

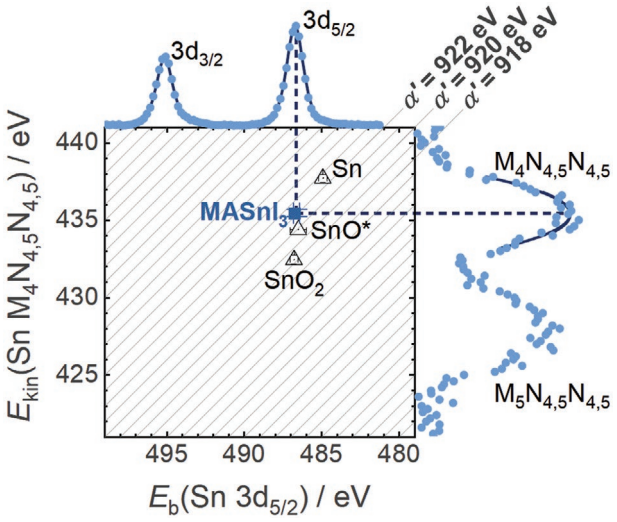


**Figure 3.** Peak identification of the Sn 3d and Sn MNN features to obtain the modified Auger parameter $\alpha'$. Maxima determination of the Sn $3d_{5/2}$ and Sn $M_4N_{4,5}N_{4,5}$ features constructs a point on the Wagner plot for a single measurement. Reference values obtained from the NIST database have been marked with an asterisk.

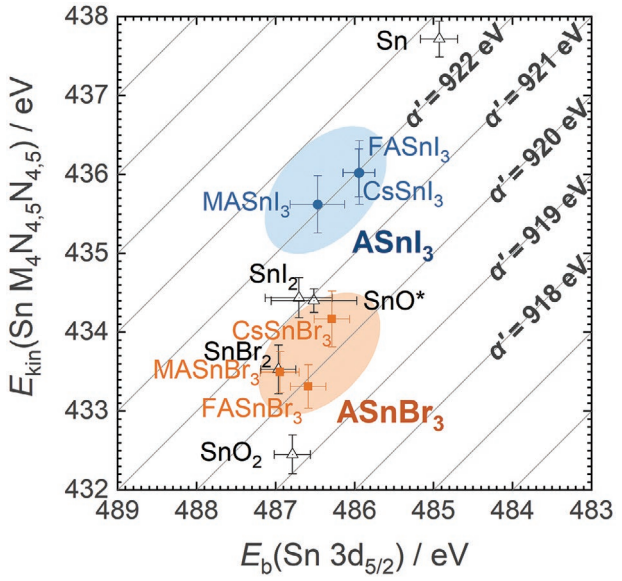


**Figure 4.** Wagner plot depicting all investigated perovskites of this study. Reference values obtained from the NIST database have been marked with an asterisk. The values depicted in this graph are summarized in Table S1 (Supporting Information) while the underlying measurement workflow is detailed in Note S1 (Supporting Information).

oxidation state for these compounds is expected to be similar. For $ASnI_3$ type perovskite however, the valence charge of the probed Sn atom would be increased over $ASnBr_3$ type perovskites due to the lowered electronegativity of the X–sites.

While this may in part explain the shift between these types of perovskites, extra-atomic relaxation effects would also contribute to the observed AP shifts. The more covalent nature of the bond for less electronegative X–sites results in increased polarizability. Similarly, for heavier halides, the expansion of the valence shell results in increased polarizability. Both factors would thus result in increased $\Delta R^{ea}$, and consequently $\alpha'$, for $ASnI_3$ type perovskites over $ASnBr_3$ type perovskites.

On the contrary, variations of the cationic A–site have minute effects on the valence charge of the B–site. Based on *ab-initio* calculations, B—A bonds in metal halides perovskites have typically been classified as ionic.[31] The performed A–site variations may merely induce distortions of the perovskite lattice that result in the tilting of the $SnX_6^{4-}$ octahedral, with negligible effects on the local Sn chemical environment. This is in line with previous reports, in which insignificant changes of the AP were reported when the structure of the material changed, but the local chemical environment (i.e., the coordination) did not.[32,33]

Furthermore, these features enable to observe the surface degradation of perovskite samples based on the change of the Sn chemical state. The herein presented references may facilitate such studies.

Following aging of the pristine perovskite samples under ambient air, the AP was determined again for each sample. Remarkable, regardless of the perovskite chemistry, all aged samples exhibit an AP at $\alpha' \approx 919$ eV, similar to the AP of $SnO_2$ according to the NIST database and verified by our own measurements (**Figure 5**a). Furthermore, the feature-richness of the Auger emission allows it to be utilized as a chemical fingerprint without the need for peak fitting. This eliminates the need for potential assumptions on the underlying processes occurring during the Auger emission. By normalizing all spectra to their maxima, the similar shape of the Auger emission for all samples becomes clear (Figure 5b). Additionally, this peak shape is highly similar to the one observed for $SnO_2$. Indeed, the decomposition of Sn-based perovskites in air has been reported to proceed through the formation of both tin (IV) oxide (i.e., $SnO_2$) and their corresponding double perovskite (i.e., $A_2SnX_6$).[6] Thus, based on the Sn chemical state alone, tin(IV) oxide as the sole degradation product of Sn on the surface for all perovskite samples could be identified, regardless of the herein employed A-, B-, or X-site chemistry. The $SnO_2$ formation at Sn-based perovskite interfaces exposed to air was recently reported based on DFT simulations.[34] Due to its hole blocking properties, its formation is often unwanted in optoelectronic devices.

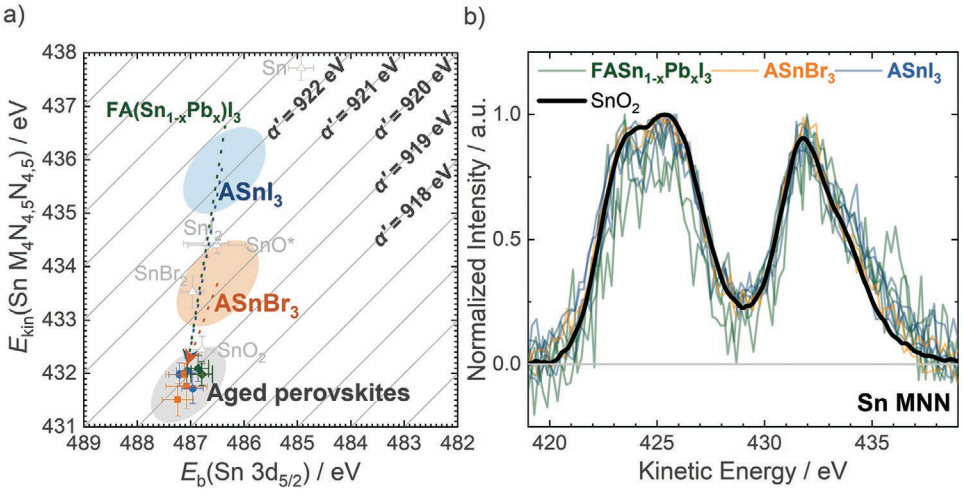


**Figure 5.** a) Wagner plot depicting $\alpha'$ for aged perovskite samples exposed to ambient conditions for multiple hours. In contrast to the pristine samples previously transferred under inert-gas, the values converge to $\alpha' \approx 919$ eV for all samples regardless of the perovskite chemistry. b) Sn MNN region of all aged perovskite samples compared to the $SnO_2$ reference following charge correction.

Based on these findings, the AP of Sn-based perovskites exhibits a high sensitivity on the Sn—halide bonding with additional dependencies on the Sn coordination and oxidation state. More recently, surface-sensitive solid state nuclear magnetic ressonance (ssNMR) spectroscopy studies on perovskites have been reported.[35] Besides the herein identified factors, the $^{119}$Sn chemical shift was identified to be also dependent on A-site variations amongst other factors.[36] As a result, the exceptionally high sensitivity of $\alpha'$ on the Sn—X bond alone makes it well-suited for selective studies on X–site variations even when multiple sites are being varied.

Consequently, these findings highlight how observation of the easily accessible Sn MNN feature can augment studies based on the Sn 3d feature alone. Combining both results in AP studies allows to eliminate issues resulting from charge referencing that are especially profound for hybrid semiconductors. Resulting shifts of $\alpha'$ are largely driven by a shift in the peak of the Sn MNN feature that highlights the higher sensitivity of the Auger emission to the chemical environment and Sn—X bond for perovskites specifically.

## 3. Conclusion

In this article, we established how AP studies can be used to perform more robust surface analysis of Sn-based perovskite surfaces using XPS. By performing comprehensive XPS analysis on high-quality reference materials, we identified the high sensitivity of $\alpha'$ on the nature of the Sn—X bond in perovskites. Additional dependencies on the Sn oxidation state were identified following aging of the perovskite samples. Due to the aforementioned vast chemical space of Sn based semiconductors, similar studies, which include additional reference materials, may aid in the more robust characterization of these compounds. Likewise, the importance of B—X bonds unraveled for Sn-based perovskites are likely to be similar for other types of perovskites.

Since no additional equipment is required for AP studies, this method can be widely adopted for the surface and interface analysis of Sn semiconductors with minimal additional effort. The high tolerance of the AP studies toward erroneous energy calibration and artifacts resulting from surface band bending makes them an ideal tool to study semiconductor surfaces and compare data sets between laboratories. Furthermore, the high sensitivity of $\alpha'$ on Sn—halide bonds makes it especially interesting to study the effects on additives affecting the X–site at perovskite interfaces. Lastly, the facile data analysis makes this method also ideal for high-throughput studies that are increasingly being adopted in the development of new semiconducting materials.

## 4. Experimental Section

*Materials*: Soda lime (25 mm × 25 mm) glasses were purchased from Advanced Election Technology Co., Ltd. Cesium iodide (CsI, 99%), methylammonium bromide (MABr, ≥98%), formamidinium bromide (FABr, ≥99%) were purchased from Tokyo Chemical Industry Co., Ltd. Methylammonium iodide (MAI, 98%), formamidinium iodide (FAI, ≥99.99%) were purchased from Greatcell Solar Ltd. Cesium bromide (CsBr, 99.999%), lead(II) iodide ($PbI_2$, 99.999%) and tin(IV) oxide ($SnO_2$, 15% $H_2O$ in colloidal dispersion) were purchased from Alfa-Aesar. Dimethyl sulfoxide (DMSO, anhydrous, 99.9%, anhydrous), dimethylformamide (DMF, 99.8% anhydrous), lead (II) thiocyanate ($Pb(SCN)_2$, (99.5%), tin(II) iodide ($SnI_2$, 99,99%), Ethyl acetate (EtOAc, 99.8%, anhydrous), tin(II) bromide ($SnBr_2$) were purchased from Sigma–Aldrich Pty Ltd. All the materials were used as received.

*Sample Preparation*: Each sample was prepared in a $N_2$-filled glove box to prevent oxidation of the used Sn(II) compounds especially. Resulting films exhibited a thickness of 100–400 nm.

*$ASnI_3$ perovskites, $ASnBr_3$ perovskites and $SnX_2$ references*: Stoichiometric amounts of A cation source chemicals (CsI, MAI, FAI, CsBr, MABr, or FABr) and corresponding B cation metal salts ($SnI_2$ or $SnBr_2$) were weighed ($H_2O$ < 0.5 ppm. $O_2$ < 0.5 ppm) and dissolved in DMSO to yield 0.3 M $CsSnI_3$, $MASnI_3$, $FASnI_3$, $CsSnBr_3$, $MASnBr_3$, $FASnBr_3$ precursors, respectively. $SnI_2$ and $SnBr_2$ were also weighed separately to get 0.3 M $SnI_2$ and $SnBr_2$ solutions in DMSO, respectively. The precursors were kept on a 75 °C hotplate during the spin-coating. The hot precursors were spin-coated onto pre-cleaned soda lime glasses at 1500 rpm with a ramp rate of 1500 rpm for 30 s, followed by a 100 °C annealing for 10 min.

$SnI_2$ and $SnBr_2$ films were prepared by only spin-coating the $SnX_2$ solutions in DMSO. Similarly, $SnO_2$ films were directly prepared from the aqueous dispersion. The annealing step was likewise performed as specified for the perovskite films.

$SnI_2$ and $SnBr_2$ films exhibited I/Sn ratios of 1.3 and 1.6, respectively, during quantification in XPS. In both cases, this ratio remained constant during each measurement taking place over multiple hours. Additionally, no further X-Ray degradation was observed during performed measurements. Therefore, changes in stoichiometry were ascribed to surface vacuum degradation during introduction of the films to the XPS chamber. Further details on the $SnBr_2$ specifically can be found in the Notes S2 (Supporting Information).

*$FA(Sn_{1-x}Pb_x)I_3$ perovskites: T*he $FASnI_3$ precursor solution was prepared by dissolving 372 mg of $SnI_2$ and 172 mg of FAI in a mix of DMF (424 µL) and DMSO (212 µL) solvents. The $FAPbI_3$ precursor solution was prepared by dissolving 461 mg $PbI_2$ and 159 mg MAI with 3.5 mol% $Pb(SCN)_2$ in 630 µL DMF and 70 µL DMSO. The two solutions were heated and dissolved at 65 °C for 2 h. Then stoichiometric amounts of $FASnI_3$ and $FAPbI_3$ perovskite precursors were mixed to obtain 1.5 M $FA(Sn_{1-x}Pb_x)I_3$ perovskites ($x$ = 0.25, 0.5, and 0.75) precursor solutions.

The perovskite films were deposited using a two-step spin coating procedure: (1) 1000 rpm for 10 s with an acceleration of 1000 rpm $s^{-1}$ and (2) 5000 rpm for 50 s with a ramp-up of 10 000 rpm $s^{-1}$. EtOAc (150 µL) was dropped onto the spinning substrate during the second spin-coating step at 20 s before the end of the procedure. The substrates were then transferred on a hotplate and annealed at 65 °C for 3 min and then 105 °C for 7 min.

*Sample Characterization*: X-ray photoelectron spectroscopy was performed in a PHI Quantum system to which samples mounted on insulating substrates were transferred using a custom-made inert-gas transfer vessel in Ar atmosphere. XPS measurements were performed at a pressure of $10^{-9}$ – $10^{-8}$ Torr. The monochromatic Al K$\alpha$ radiation was generated from an electron beam at a power of 12.6 W and a voltage of 15 kV. To minimize beam damage during measurements, the beam spot with a diameter of 50 µm was continuously scanned over an area of 500 × 1000 µm$^2$. Charge neutralization was performed using a low-energy electron source. Short-term measurements (<1 min) of the Sn 3d core level before and after each presented long-term measurement (≈30 min) were conducted to rule out changes in the chemical state due to X-ray induced beam damage. Peak fitting of photoelectron features was performed in Casa XPS using Voigt profiles with GL ratios of 60 following Shirley-background subtraction. Due to the low binding energy shift, a single component was used for non-metallic XPS features. In cases where a Sn(0) feature was present, an additional component was used. For Auger electron features, the area around the peak was fitted using a cubic function, a visual description of this method can be found in Note 3 (Supporting Information). The binding energy scale was referenced to

the main component of adventitious carbon at 284.8 eV, resulting in a typical inaccuracy of ±0.2 eV. For each measured composition, two areas on the same sample were measured to assess materials variations across the sample. Resulting measurement values were then averaged and the error $\Delta E$ for the feature maxima on the binding and kinetic energies scale was calculated according to

$$\Delta E = \pm\left(\frac{|E_1 - E_2|}{2} + 0.2\ \text{eV}\right) \quad (3)$$

where $E_1$ and $E_2$ denote the measured energy values for the areas 1 and 2 on each measured samples. The additional 0.2 eV accounts for the potential systematic error introduced through charge referencing. The error for the modified Auger parameter is smaller, as it is not affected by this additional uncertainty.

Atomic ratios were calculated using the instrument specific relative sensitivity factors. To estimate the information depth depending on the observed feature, the inelastic mean free path (IMFP) was calculated from the kinetic energy of the detected electrons based on the Tanuma, Powell, and Penn formula.[37] A detailed descripted of the XPS characterization workflow for the herein investigated Sn-based perovskites can be found in the Note S1 (Supporting Information).

XRD analysis was performed in a Bruker D8 Discovery diffractometer using Cu k$\alpha$ radiation in Bragg-Brentano geometry. The full conversion of each Sn-based perovskite sample to the perovskite phase was confirmed by the absence of signals related to $SnI_2$ or $SnBr_2$.

## Supporting Information

Supporting Information is available from the Wiley Online Library or from the author.

## Acknowledgements

All authors acknowledge funding from the the Strategic Focus Area–Advanced Manufacturing (SFA–AM) through the project Advancing manufacturability of hybrid organic–inorganic semiconductors for large area optoelectronics (AMYS). A.W. acknowledges Jyotish Patidar for his support with the XRD measurement setup. H. L. thanks the funding of China Scholarship Council (CSC) from the Ministry of Education of P. R. China.

## Conflict of Interest

The authors declare no conflict of interest.

## Author Contributions

Conceptualization and design of the study was performed by A.W., F.F., and S.S. Synthesis of the reference materials was performed by H.L. and J.P. under supervision of F.F. XPS analysis, as well as XRD analysis of the reference materials was performed by A.W. under supervision of S.S. Analysis and interpretation of the XPS results was performed by A.W. and S.S. A.W. wrote the initial draft of the manuscript with contributions from S.S. All authors edited and contributed to the final version of the manuscript. All authors have given approval to the final version of the manuscript.

## Data Availability Statement

The data that support the findings of this study are available in the supplementary material of this article.

## Keywords

Auger parameter, semiconductors, Sn perovskites, Wagner plot, XPS

Received: August 18, 2022
Revised: November 18, 2022
Published online: December 9, 2022

[1] J. Andrade-Arvizu, R. F. Rubio, V. Izquierdo-Roca, I. Becerril-Romero, D. Sylla, P. Vidal-Fuentes, Z. J. Li-Kao, A. Thomere, S. Giraldo, K. Tiwari, S. Resalati, M. Guc, M. Placidi, *ACS Appl. Mater. Interfaces* **2022**, *14*, 1177.
[2] W. Shi, M. Gao, J. Wei, J. Gao, C. Fan, E. Ashalley, H. Li, Z. Wang, *Adv. Sci.* **2018**, *5*, 1700602.
[3] S. An, Y. Liao, M. Kim, *ACS Appl. Mater. Interfaces* **2021**, *13*, 61396.
[4] W. Yang, F. Igbari, Y. Lou, Z. Wang, L. Liao, *Adv. Energy Mater.* **2020**, *10*, 1902584.
[5] M. M. Byranvand, W. Zuo, R. Imani, M. Pazoki, M. Saliba, *Chem. Sci.* **2022**, *13*, 6766.
[6] L. Lanzetta, T. Webb, N. Zibouche, X. Liang, D. Ding, G. Min, R. J. E. Westbrook, B. Gaggio, T. J. Macdonald, M. S. Islam, S. A. Haque, *Nat. Commun.* **2021**, *12*, 2853.
[7] D. Yun, S. Lee, S. H. Kim, C. Jung, Y. S. Kim, J. G. Chung, S. Heo, Y. Kwon, E. Lee, J. Kim, D. Ko, S. Y. Kim, *Small Methods* **2021**, *5*, 2001264.
[8] C. Das, M. Wussler, T. Hellmann, T. Mayer, I. Zimmermann, C. Maheu, M. K. Nazeeruddin, W. Jaegermann, *ACS Appl. Mater. Interfaces* **2020**, *12*, 40949.
[9] G. Greczynski, L. Hultman, *Sci. Rep.* **2021**, *11*, 11195.
[10] F. Zu, C. M. Wolff, M. Ralaiarisoa, P. Amsalem, D. Neher, N. Koch, *ACS Appl. Mater. Interfaces* **2019**, *11*, 21578.
[11] G. Teeter, S. P. Harvey, C. L. Perkins, K. Ramanathan, I. L. Repins, *J Vac Sci Technol A* **2019**, *37*, 031202.
[12] T. C. Taucher, I. Hehn, O. T. Hofmann, M. Zharnikov, E. Zojer, *J. Phys. Chem. C* **2016**, *120*, 3428.
[13] L. Kövér, G. Moretti, Z. Kovács, R. Sanjinés, I. Cserny, G. Margaritondo, J. Pálinkás, H. Adachi, *J. Vac. Sci. Technol., A* **1995**, *13*, 1382.
[14] S. W. Gaarenstroom, N. Winograd, *J. Chem. Phys.* **1977**, *67*, 3500.
[15] G. Moretti, *J Electron Spectros Relat Phenomena* **1998**, *95*, 95.
[16] G. Moretti, *Surf. Interface Anal.* **1990**, *16*, 159.
[17] M. C. Biesinger, L. W. M. Lau, A. R. Gerson, R. S. C. Smart, *Phys. Chem. Chem. Phys.* **2012**, *14*, 2434.
[18] J. L. Bourque, M. C. Biesinger, K. M. Baines, *Dalton Trans.* **2016**, *45*, 7678.
[19] T. Liu, X. Zhao, J. Li, Z. Liu, F. Liscio, S. Milita, B. C. Schroeder, O. Fenwick, *Nat. Commun.* **2019**, *10*, 1.
[20] S. Siol, J. Mann, J. Newman, T. Miyayama, K. Watanabe, P. Schmutz, C. Cancellieri, L. P. H. Jeurgens, *Surf. Interface Anal.* **2020**, *52*, 802.
[21] M. A. Muñoz-Márquez, M. Zarrabeitia, E. Castillo-Martínez, A. Eguía-Barrio, T. Rojo, M. Casas-Cabanas, *ACS Appl. Mater. Interfaces* **2015**, *7*, 7801.
[22] P. Schulz, D. Cahen, A. Kahn, *Chem. Rev.* **2019**, *119*, 3349.
[23] A. V. Naumkin, A. Kraut-Vass, S. W. Gaarenstroom, C. J. Powell, "NIST X-ray Photoelectron Spectroscopy Database, NIST Standard Reference Database Number 20, National Institute of Standards and Technology, Gaithersburg MD, **2000**, https://doi.org/10.18434/T4T88K.
[24] M. A. Stranick, A. Moskwa, *Surf. Sci. Spectra* **1993**, *2*, 45.
[25] M. A. Stranick, A. Moskwa, *Surf. Sci. Spectra* **1993**, *2*, 50.
[26] T. W. Haas, J. T. Grant, G. J. Dooley, *J. Appl. Phys.* **1972**, *43*, 1853.
[27] A. F. Lee, R. M. Lambert, *Phys. Rev. B* **1998**, *58*, 4156.
[28] J. A. Taylor, S. M. Merchant, D. L. Perry, *J. Appl. Phys.* **1995**, *78*, 5356.

[29] V. M. Jiménez, J. A. Mejías, J. P. Espinós, A. R. González-Elipe, *Surf. Sci.* **1996**, *366*, 545.
[30] C. D. Wagner, *J Electron Spectros Relat Phenomena* **1977**, *10*, 305.
[31] M. Wuttig, C. Schön, M. Schumacher, J. Robertson, P. Golub, E. Bousquet, C. Gatti, J. Raty, *Adv. Funct. Mater.* **2022**, *32*, 2110166.
[32] P. C. Snijders, L. P. H. Jeurgens, W. G. Sloof, *Surf. Sci.* **2005**, *589*, 98.
[33] S. Zhuk, S. Siol, *Appl. Surf. Sci.* **2022**, *601*, 154172.
[34] A. Morteza Najarian, M. Vafaie, A. Johnston, T. Zhu, M. Wei, M. I. Saidaminov, Y. Hou, S. Hoogland, F. P. García de Arquer, E. H. Sargent, *Nat. Electron.* **2022**, *5*, 511.
[35] L. Piveteau, V. Morad, M. V. Kovalenko, *J. Am. Chem. Soc.* **2020**, *142*, 19413.
[36] D. J. Kubicki, D. Prochowicz, E. Salager, A. Rakhmatullin, C. P. Grey, L. Emsley, S. D. Stranks, *J. Am. Chem. Soc.* **2020**, *142*, 7813.
[37] H. Shinotsuka, S. Tanuma, C. J. Powell, D. R. Penn, *Surf. Interface Anal.* **2015**, *47*, 871.